Supporting Information

Upcycling spent cathodes into single-crystalline Ni-rich cathode materials through selective lithium extraction

Kyoung Sun Kim[a,b], Min Ku Jeon[c], Seok Hyun Song[a,b], Seokjae Hong[a,b], Hwa Soo Kim[d], Sung-Wook Kim[c], Jinsoo Kim[e], Pilgun Oh[f], Junhyeok Hwang[g], Jinju Song[h], Jiyoung Ma[h], Jung-Je Woo[h], Seung-Ho Yu[b], Hyungsub Kim[a*]

K. S. Kim, S. H. Song, S. Hong, Dr. H. Kim

[a] *Neutron Science Division, Korea Atomic Energy Research Institute (KAERI), 111 Daedeok-daero 989 Beon-Gil, Yuseong-gu, Daejeon 34057, Republic of Korea*

*Corresponding author: Hyungsub Kim (*hyungsubkim@kaeri.re.kr*)

K. S. Kim, S. H. Song, S. Hong, Prof. S.-H. Yu

[b] *Department of Chemical and Biological Engineering, Korea University, 145 Anam-Ro, Seongbuk-Gu, Seoul 02841, Republic of Korea*

.

Dr. M. K. Jeon, Dr. S.-W. Kim

[c] *Decommissioning Technology Division, Korea Atomic Energy Research Institute (KAERI), 111 Daedeok-daero 989 Beon-Gil, Yuseong-gu, Daejeon 34057, Republic of Korea*

H. S. Kim

[d] *Department of Robotics and Mechatronics Engineering, Daegu Gyeongbuk Institute of Science and Technology (DGIST), Daegu 42988, Republic of Korea*

Dr. J. Kim

[e] *Ulsan Advanced Energy Technology R&D Center, Korea Institute of Energy Research (KIER), Ulsan 44776, Republic of Korea*

Prof. P. Oh

[f] *Department of Nanotechnology Engineering, Pukyong National University, 45 Yongso-ro, Nam-gu, Busan 48547, Republic of Korea*

J. Hwang

[g] *Department of Smart Green Technology Engineering, Pukyong National University, 45 Yongso-ro, Nam-gu, Busan 48547, Republic of Korea*

Dr. J. Song, Dr. J. Ma, Dr. J.-J. Woo

[h] *Gwangju Clean Energy Research Center, Korea Institute of Energy Research (KIER), 270-25 Samso-ro, Buk-gu, Gwangju 61003, Republic of Korea*

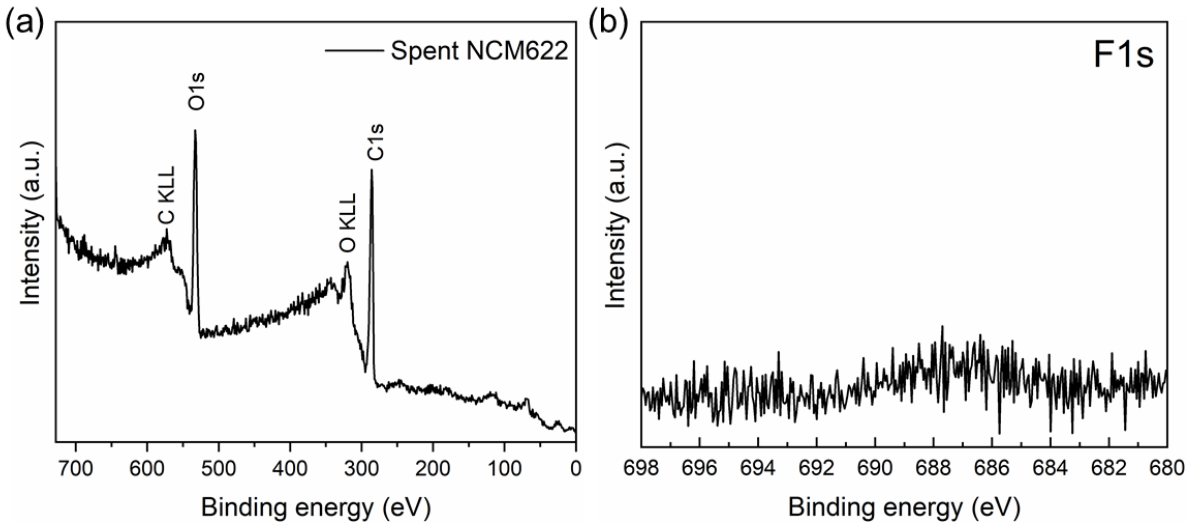

Fig. S1 (a) Wide scan and (b) F 1s of X-ray photoelectron spectra of spent $LiNi_{0.6}Co_{0.2}Mn_{0.2}O_2$ (NCM622).

Sample	Carbon (*wt.*%)	Deviation
Spent NCM622	0.089	0.00653

Table S1 Carbon content of spent NCM622 obtained from a carbon determinator.

	Li	Ni	Co	Mn
Spent NCM622	0.98	0.584	0.21	0.206
Commercial NCM622	1.164	0.601	0.203	0.196

Table S2 Lithium, nickel, cobalt, and manganese content in spent and commercial NCM622 analyzed using inductively coupled plasma-mass spectrometry (ICP-MS).

Spent NCM622	***Layered NCM622* (*R-3m*)**	**$Ni(OH)_2$ (*P-3m1*)**
a (Å)	2.86996 (4)	3.046 (1)
c (Å)	14.2272 (2)	4.594 (1)
Vol. (Å^3)	101.484 (3)	36.91 (2)
Phase fraction (*wt.*%)	96.9 (7)	3.1 (1)
R_p (%)	2.43	
R_{wp} (%)	3.24	

Spent NCM622	***x***	***y***	***z***	**B_{iso}**	***Occ.***
Li1	0	0	0	0.87 (2)	0.961 (1)
Ni1	0	0	0	0.87 (2)	0.039 (1)
Ni2	0	0	0.5	0.36 (2)	0.552 (1)
Co1	0	0	0.5	0.36 (2)	0.212
Mn1	0	0	0.5	0.36 (2)	0.207
Li2	0	0	0.5	0.36 (2)	0.029 (1)
O1	0	0	0.24156 (6)	0.86 (2)	1.0

Table S3 Detailed structure information from Rietveld refinement of neutron diffraction (ND) pattern of spent NCM622.

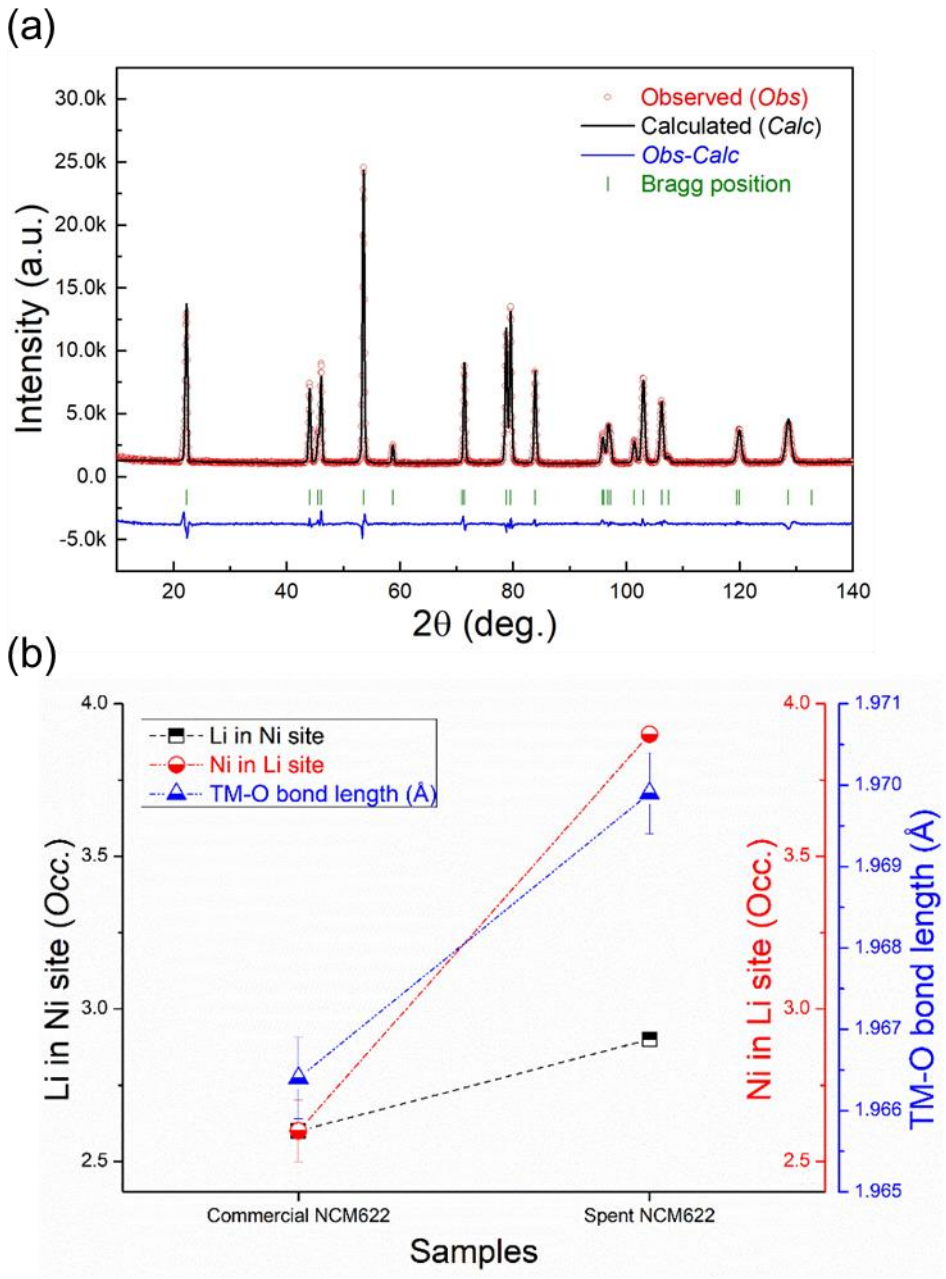

Fig. S2 (a) Rietveld refinement of ND pattern of commercial NCM622. (b) Comparison of Li–Ni intermixing and TM–O bond length between spent and commercial NCM622.

Commercial NCM622	***Layered NCM622* (*R-3m*)**
a (Å)	2.86767 (3)
c (Å)	14.2253 (2)
Vol. (Å^3)	101.310 (2)
R_p (%)	3.51
R_{wp} (%)	5.03
R_I (%)	2.15
R_F (%)	1.39

Commercial NCM622	***x***	***y***	***z***	**B_{iso}**	***Occ.***
Li1	0	0	0	0.96 (2)	0.974 (1)
Ni1	0	0	0	0.96 (2)	0.026 (1)
Ni2	0	0	0.5	0.29 (2)	0.574 (1)
Co1	0	0	0.5	0.29 (2)	0.2
Mn1	0	0	0.5	0.29 (2)	0.2
Li2	0	0	0.5	0.29 (2)	0.026 (1)
O1	0	0	0.2413 (1)	0.65 (2)	1.0

Table S4 Detailed structure information from Rietveld refinement of ND pattern of commercial NCM622.

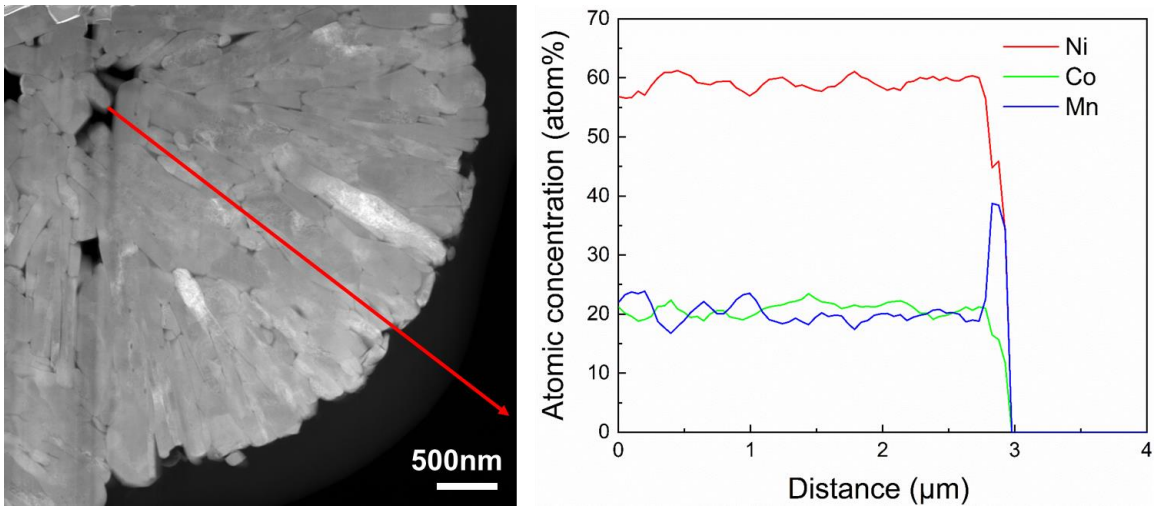

Fig. S3 Cross-sectional transmission electron microscopy (TEM) image and elemental atomic concentration profile of spent NCM622 from TEM-energy dispersive X-ray spectroscopy (EDS) line scan.

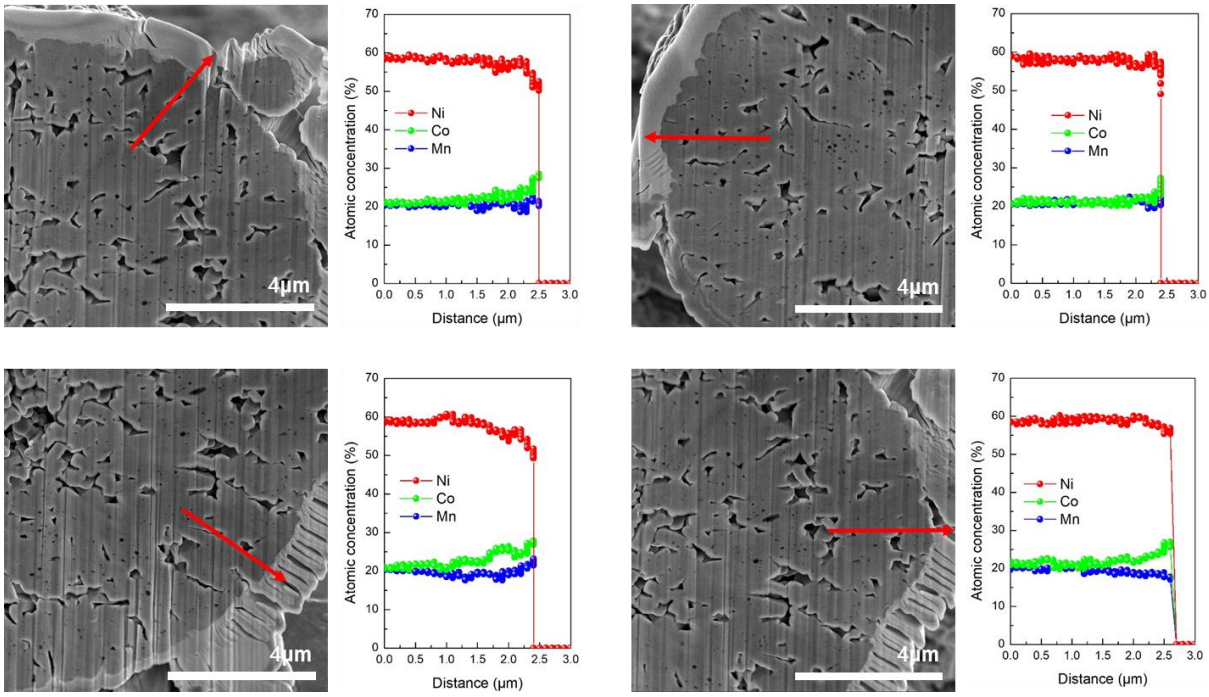

Fig. S4 Cross-sectional scanning electron microscopy (SEM) images and elemental atomic concentration profiles of spent NCM622 from SEM-EDS line scan.

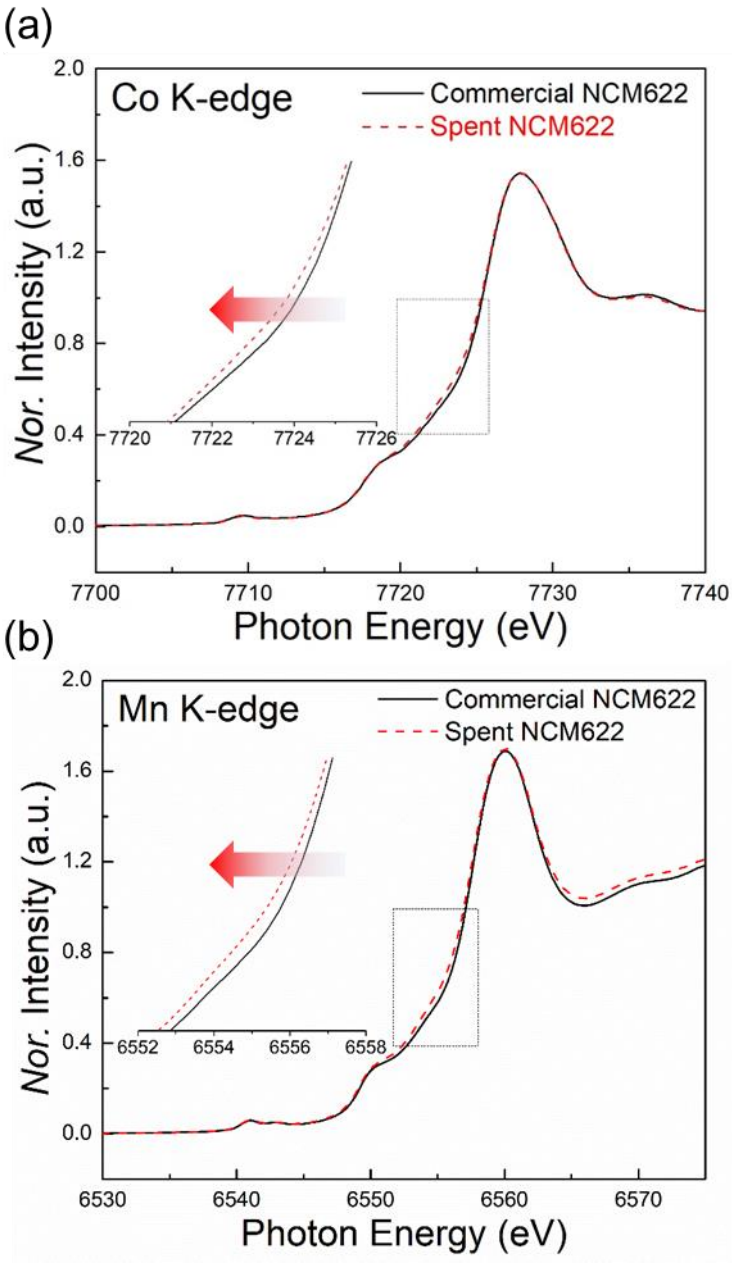

Fig. S5 (a) Co K-edge and (b) Mn K-edge X-ray absorption near edge structure (XANES) spectra of commercial and spent NCM622.

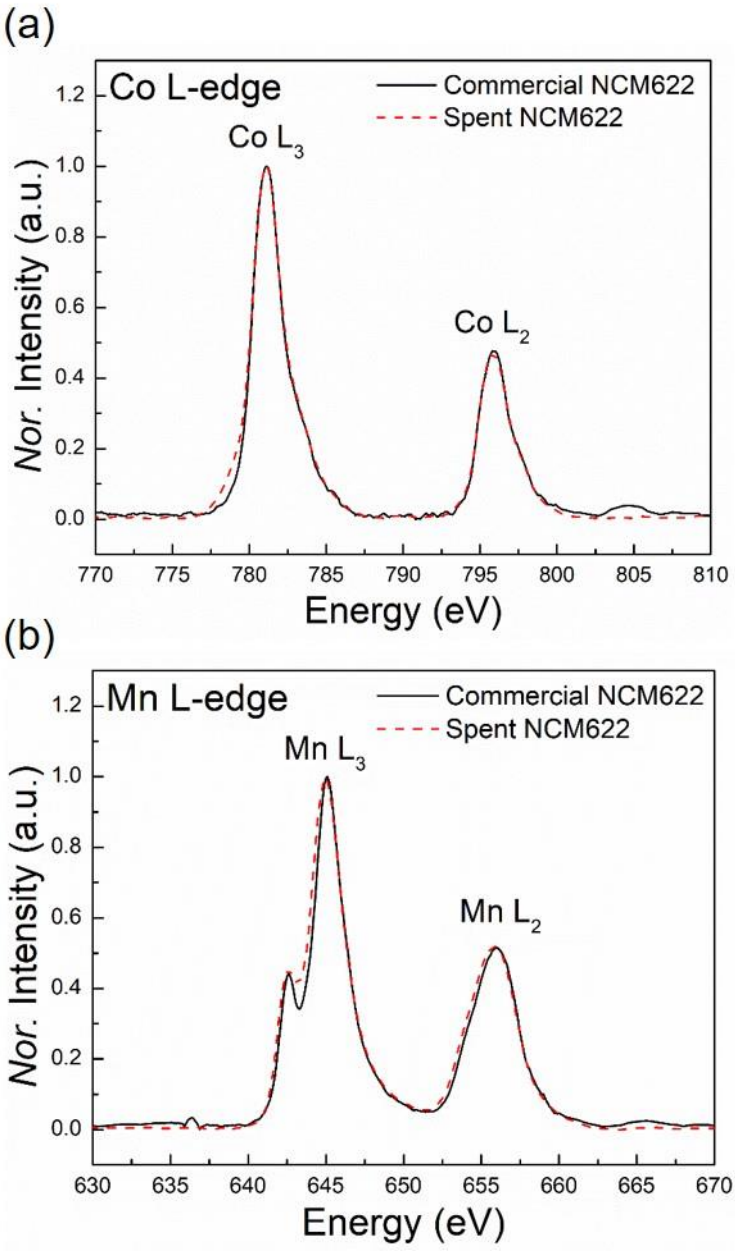

Fig. S6 (a) Co L-edge and (b) Mn L-edge soft X-ray absorption spectroscopy (XAS) spectra of commercial and spent NCM622.

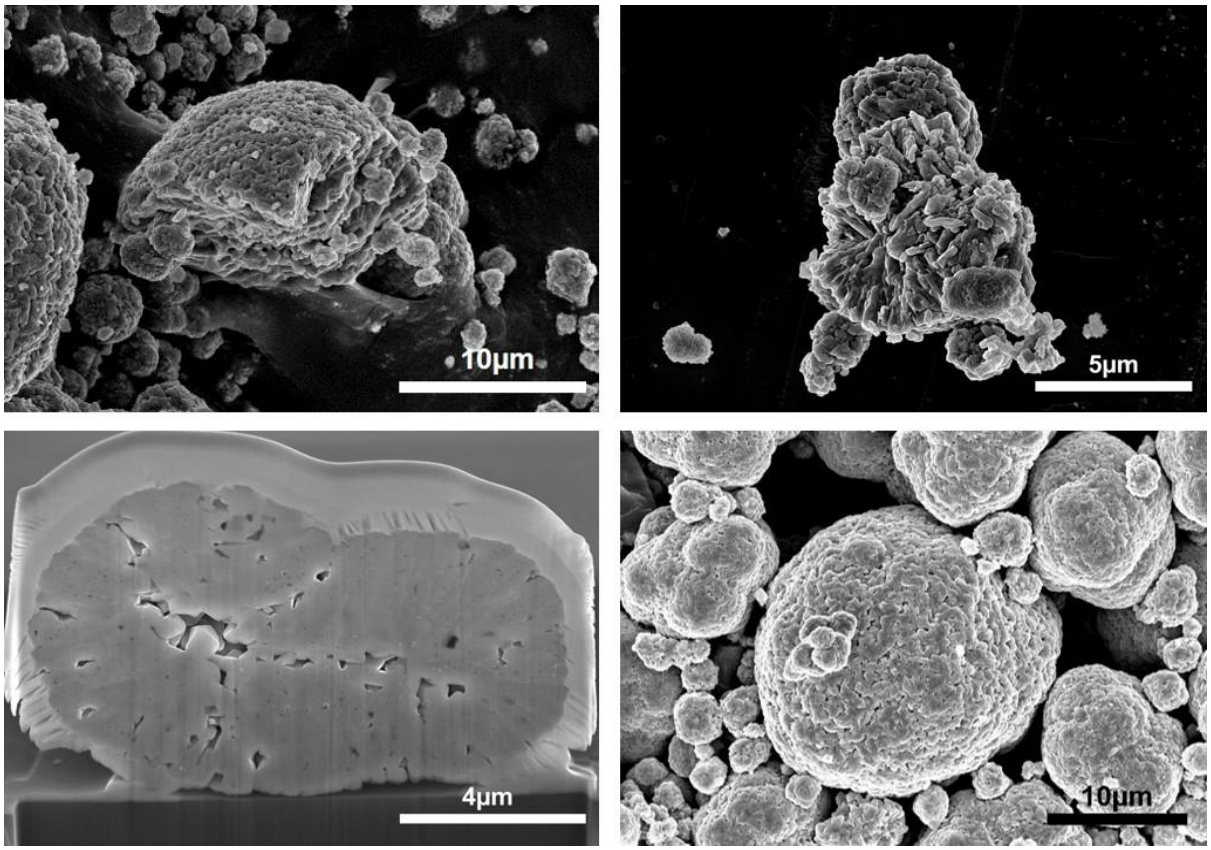

Fig. S7 SEM images of spent NCM622.

	Li	Ni	Co	Mn
Chlorinated NCM622	0.028	0.554	0.232	0.214

Table S5 Lithium, nickel, cobalt, and manganese content in chlorinated NCM622 analyzed using ICP-MS.

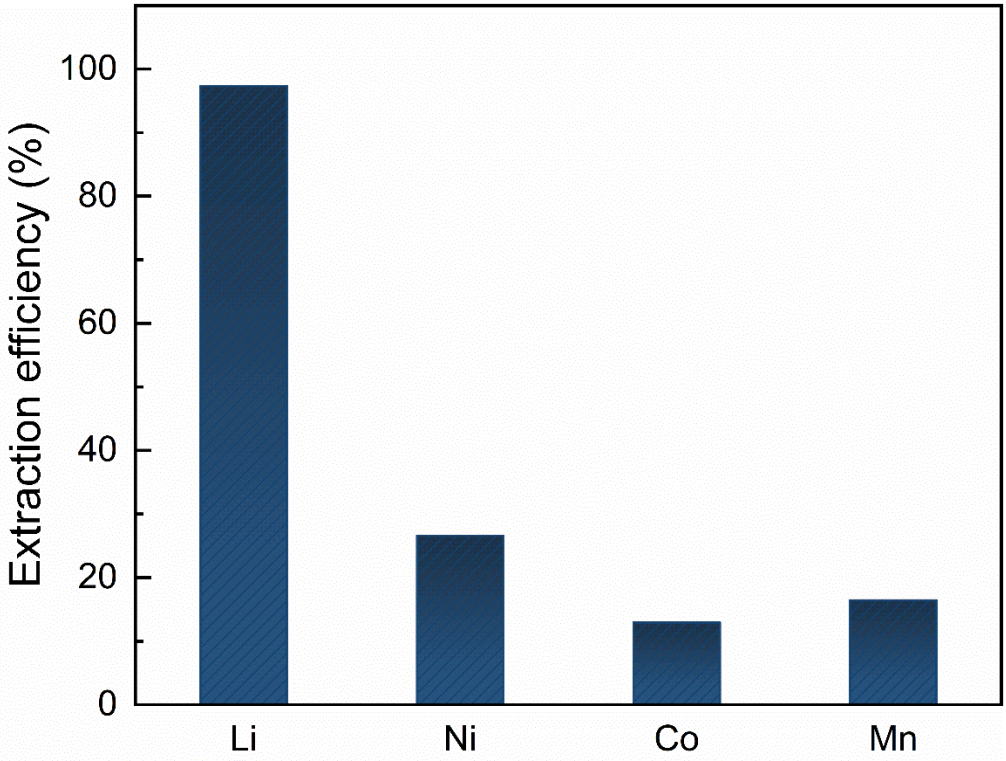

Fig. S8 Efficiency of lithium, nickel, cobalt, and manganese extraction during chlorination.

The extraction efficiencies for both lithium and transition metals were determined using ICP-MS results, with a focus on characterizing the solubilized transition metals. The formula to calculate the extraction efficiency is presented in Equation (1).[1]

$$(1)\ Extraction\ \ efficiency\ \ (\%)\ \ = \left(m_f w f_x / m_i\right)\ \times\ 100\%$$

In this equation, wf_x represents the final mass fraction of x (where X could be Li, Ni, Co, or Mn), m_f is the final extracted mass, and m_i is the initial mass.

The selectivity in extracting metal ions is largely influenced by the bond strength (or bond length) between the metal ions and oxygen within the crystal structure, and it is also influenced by the overall composition of the compound. For the spent cathode, which consists of a mixture of lithium, nickel, cobalt, and manganese, it has been reported that the bond length between metal ions and oxygen follows the sequence Li-O > Ni-O > Co-O > Mn-O.[2] Consequently, lithium becomes the foremost element to be extracted. While conditions such as temperature and time might vary from $LiNi_xCo_yMn_{1-x-y}O_2$ during the extraction reaction of standard metal oxides (TM_xO_y), the intrinsic reaction mechanism remains unchanged.[3-5] The chlorination reaction involving transition metal oxides and chlorine gas is depicted in Equation (2).

(2) $TM_xO_y \;+\; xCl_2 \;\rightarrow xTMCl_2 + (^{y}/_{2})O_2$

Sample	Purity (%)
Purified-LiCl	98.4

Table S6 Purity of LiCl after removing chlorinated transition metals using Na_2CO_3.

Based on the ICP-MS results, the purity was determined through Equation (3). In Equation (3) below, wf_x is the final mass fraction of X (Li, Ni, Co, or Mn).

$$(3)\ Purity\ (\%) = \left(\frac{wf_{Li}}{wf_{Li}+wf_{Ni}+wf_{Co}+wf_{Mn}}\right) \times 100\%$$

Chlorinated NCM622	M_3O_4 (Fd-3m)	M_7O_8 (Fm-3m)	MO (Fm-3m)
a (Å)	8.2380 (7)	8.2904 (4)	4.1459 (1)
Vol. (Å^3)	559.06 (8)	569.80 (5)	71.264 (4)
Phase fraction *(wt.%)*	55.81 (2)	20.39 (1)	23.80 (1)
R_I (%)	7.09	5.23	2.39
R_F (%)	4.08	3.48	1.51
R_p (%)		3.99	
R_{wp} (%)		5.19	

M_3O_4 (Fd-3m)	*x*	*y*	*z*	B_{iso}	*Occ.*
Ni1	0	0	0	1.0_{fix}	0.58
Co1	0	0	0	1.0_{fix}	0.05
Mn1	0	0	0	1.0_{fix}	0.37
Ni2	0.375	0.375	0.375	1.0_{fix}	0.23
Co2	0.375	0.375	0.375	1.0_{fix}	0.77
O1	0.2687 (3)	0.2687 (3)	0.2687 (3)	1.5_{fix}	1.0

M_7O_8 (Fm-3m)	*x*	*y*	*z*	B_{iso}	*Occ.*
Ni1	0	0	0	1.0_{fix}	0.13
Mn1	0	0	0	1.0_{fix}	0.87
Ni2	0	0.25	0.25	1.0_{fix}	0.96
Mn2	0	0.25	0.25	1.0_{fix}	0.04
O1	0.25	0.25	0.25	1.5_{fix}	1.0
O2	0.2173 (8)	0	0	1.5_{fix}	1.0

MO (Fm-3m)	*x*	*y*	*z*	B_{iso}	*Occ.*
Ni1	0	0	0	1.0_{fix}	0.62
Co1	0	0	0	1.0_{fix}	0.38
O1	0.5	0.5	0.5	1.5_{fix}	1.0

Table S7 Detailed structure information from Rietveld refinement of ND pattern of chlorinated NCM622.

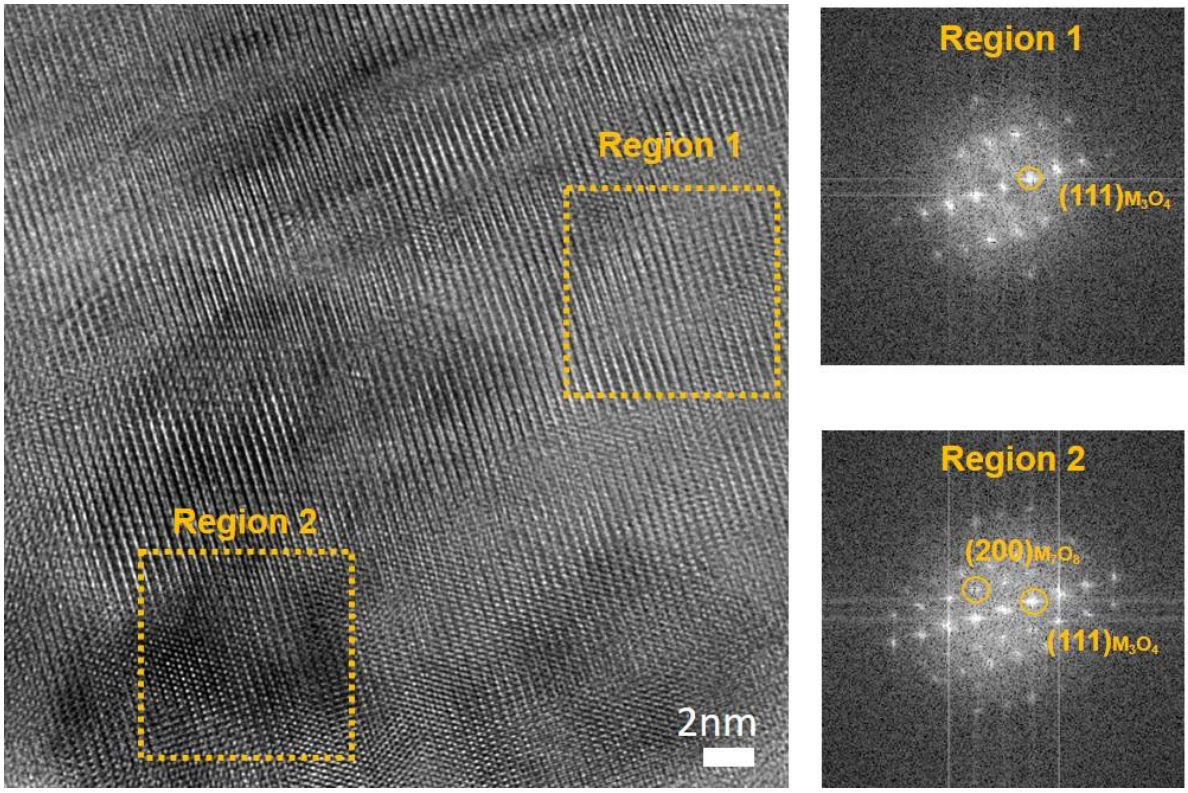

Fig. S9 TEM images of chlorinated NCM622 and Fourier transforms of the regions enclosed by the yellow-dotted lines.

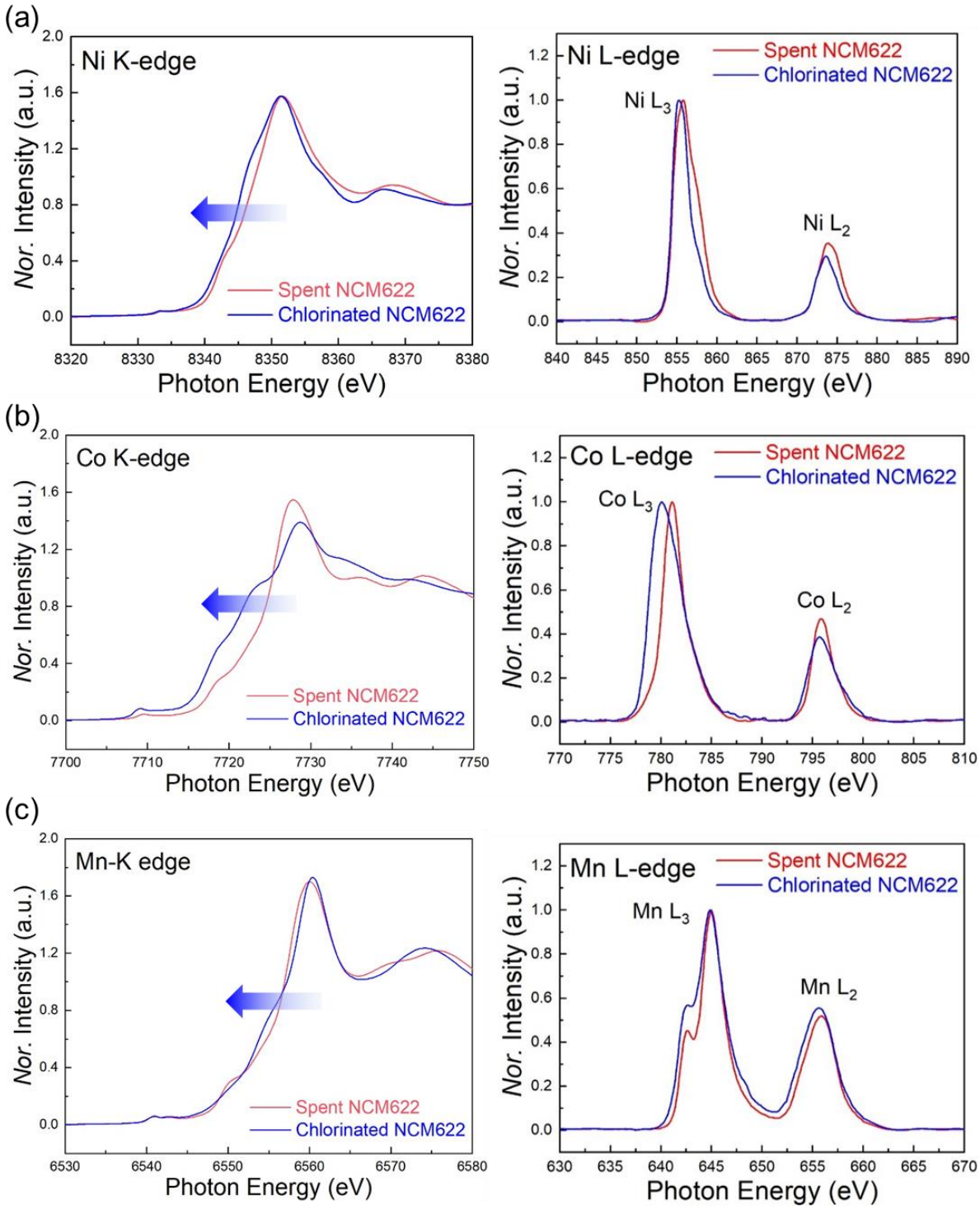

Fig. S10 XANES and soft-XAS spectra of (a) Ni K-edge/L-edge, (b) Co K-edge/L-edge, and (c) Mn K-edge/L-edge of spent and chlorinated NCM622.

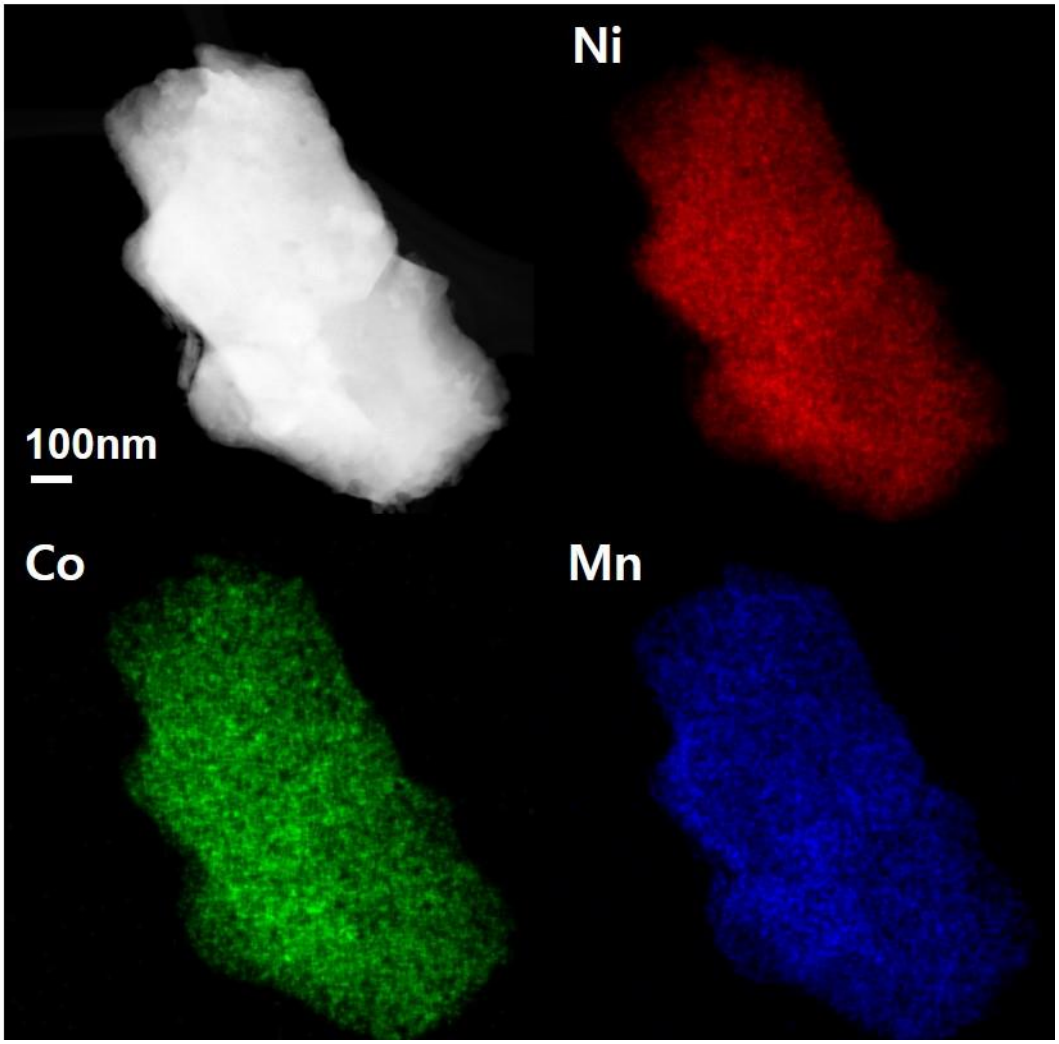

Fig. S11 TEM–EDS mapping images of chlorinated NCM622.

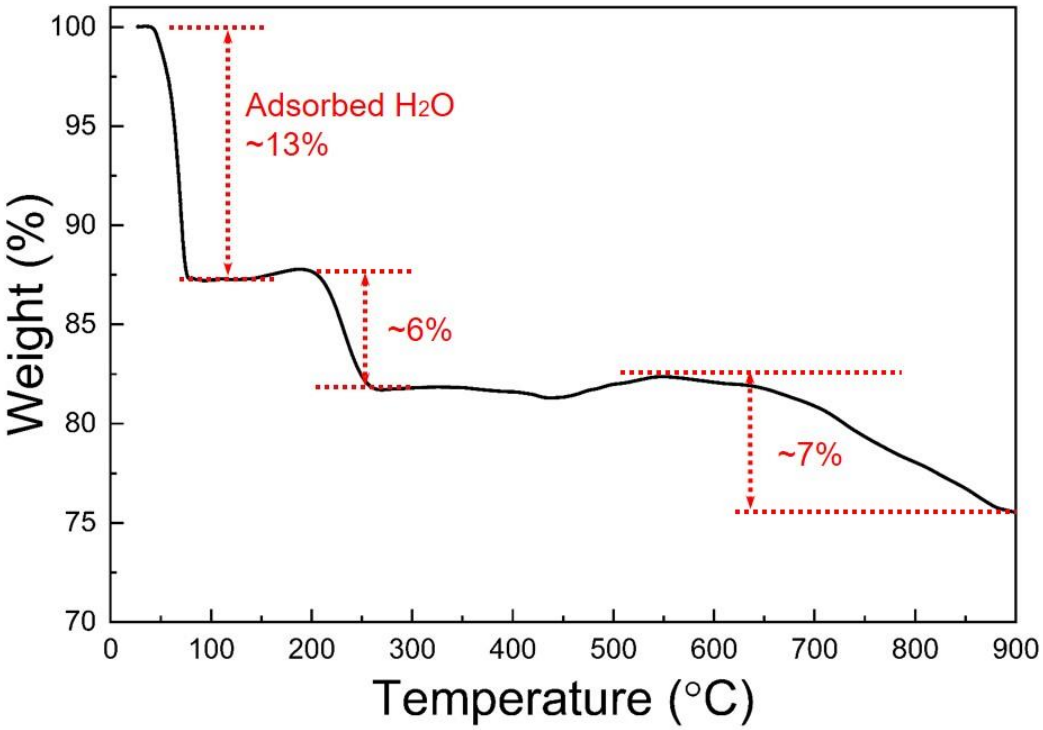

Fig. S12 Thermogravimetric analysis (TGA) of the precursor mixture consisting of chlorinated NCM622, $LiOH \cdot H_2O$, and $Ni(OH)_2$.

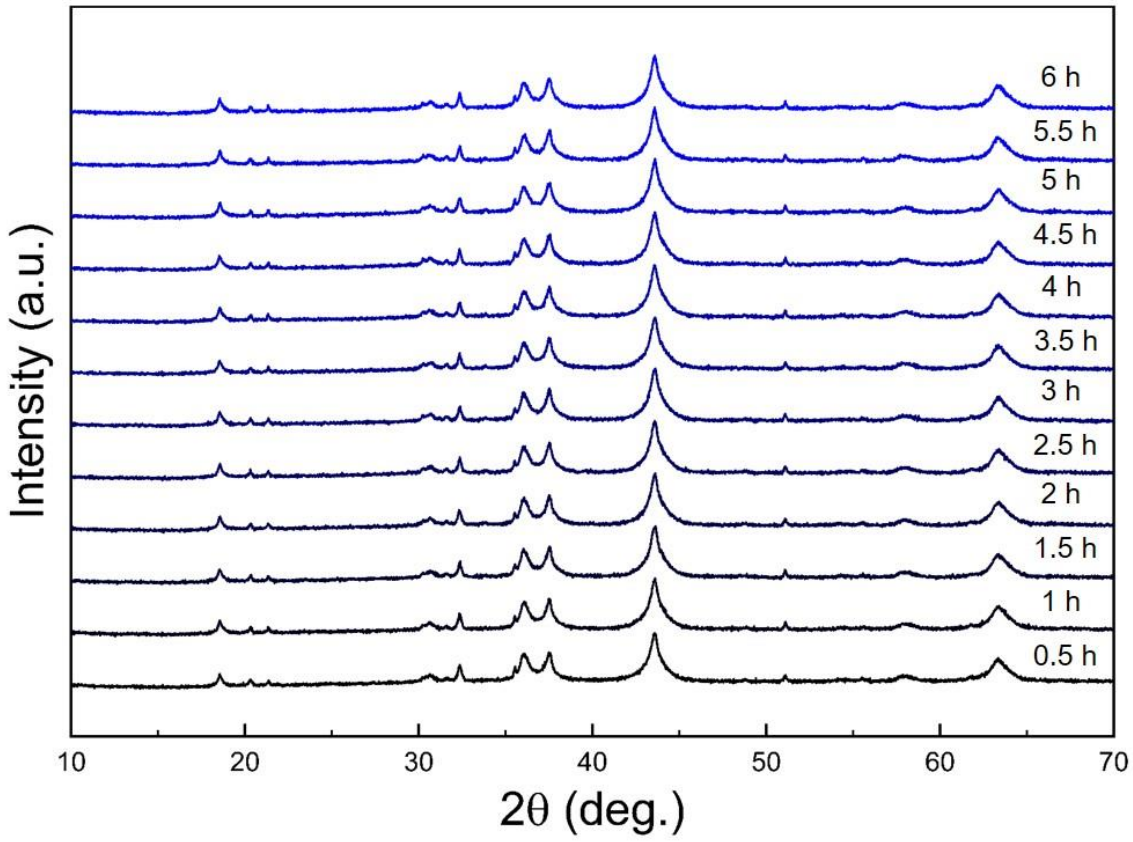

Fig. S13 *In situ* high-temperature X-ray diffraction (HT-XRD) patterns of precursor mixture during pre-aging at 250°C for 6 h.

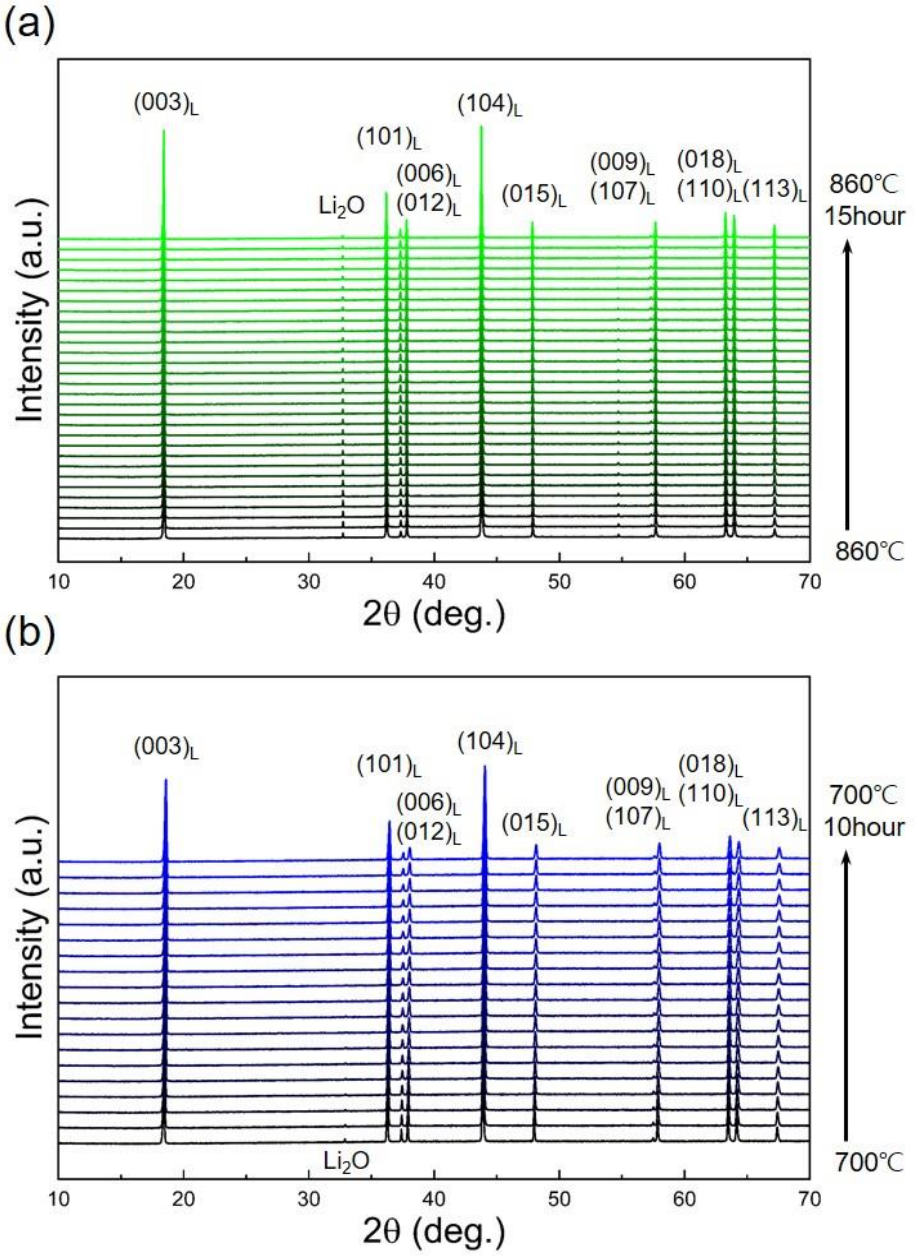

Fig. S14 *In situ* HT-XRD patterns of precursor mixture during aging at (a) 860°C for 15 h and (b) 700°C for 10 h.

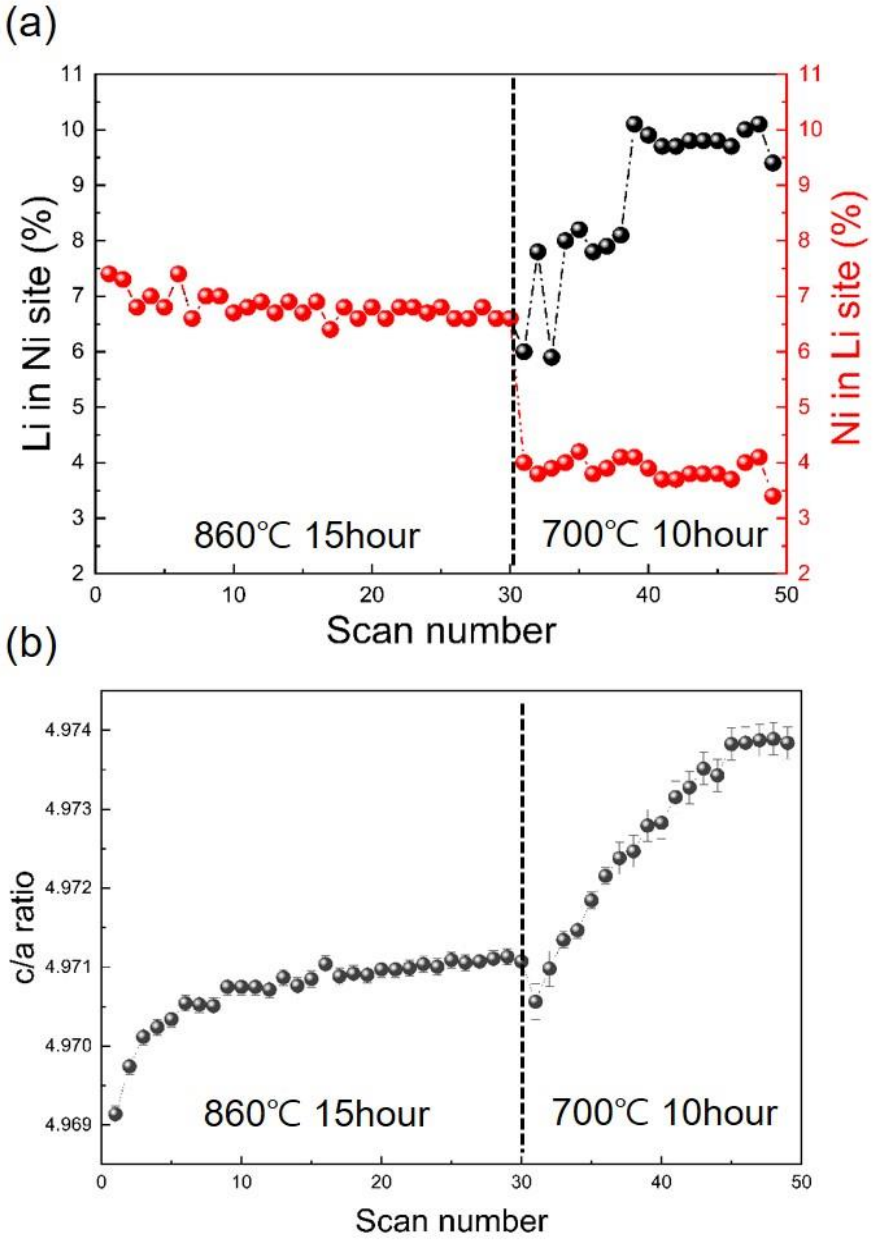

Fig. S15 (a) Li–Ni intermixing and (b) c/a ratio changes during aging at 860°C for 15 h and 700°C for 10 h analyzed from Rietveld refinement of *in situ* HT-XRD patterns.

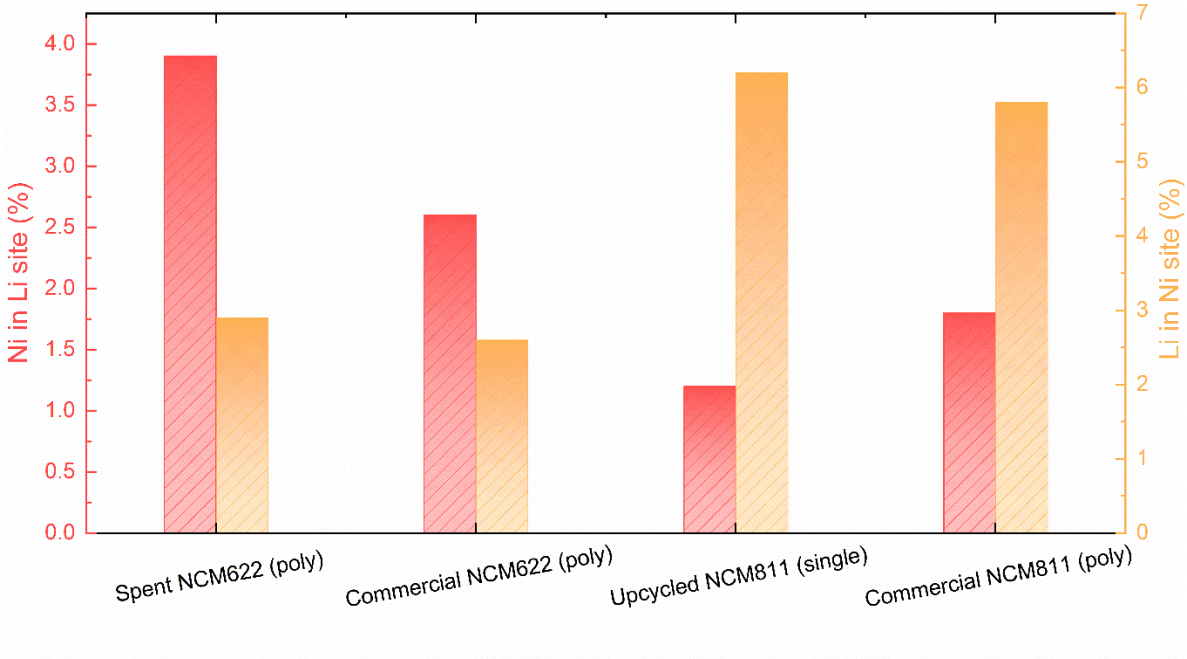

Fig. S16 Extent of Li-Ni intermixing in spent NCM622, commercial NCM622, single-crystalline upcycled $LiNi_{0.8}Co_{0.1}Mn_{0.1}O_2$ (NCM811), and poly-crystalline commercial NCM811, as derived from Rietveld refinement of ND patterns.

Upcycled NCM811	***Layered NCM811* (*R-3m*)**
a (Å)	2.87030 (4)
c (Å)	14.2035 (2)
Vol. (Å^3)	101.339 (2)
R_p (%)	3.78
R_{wp} (%)	5.42
R_I (%)	1.36
R_F (%)	1.17

Upcycled NCM811	***x***	***y***	***z***	**B_{iso}**	***Occ.***
Li1	0	0	0	1.0 (1)	0.988 (1)
Ni1	0	0	0	1.0 (1)	0.012 (1)
Ni2	0	0	0.5	0.28 (2)	0.746 (1)
Co1	0	0	0.5	0.28 (2)	0.100 (0)
Mn1	0	0	0.5	0.28 (2)	0.092 (0)
Li2	0	0	0.5	0.28 (2)	0.062 (1)
O1	0	0	0.24147 (6)	0.96 (3)	1.0

Commercial NCM811	***Layered NCM811* (*R-3m*)**
a (Å)	2.87224 (3)
c (Å)	14.1990 (2)
Vol. (Å^3)	101.444 (2)
R_p (%)	3.72
R_{wp} (%)	6.05
R_I (%)	1.57
R_F (%)	1.11

Commercial NCM811	***x***	***y***	***z***	**B_{iso}**	***Occ.***
Li1	0	0	0	1.0 (1)	0.982 (1)
Ni1	0	0	0	1.0 (1)	0.018 (1)
Ni2	0	0	0.5	0.21 (2)	0.750 (2)
Co1	0	0	0.5	0.21 (2)	0.096
Mn1	0	0	0.5	0.21 (2)	0.096
Li2	0	0	0.5	0.21 (2)	0.058 (2)
O1	0	0	0.24138 (6)	0.99 (3)	1.0

Table S8 Detailed structure information from Rietveld refinement of ND patterns of upcycled and commercial NCM811.

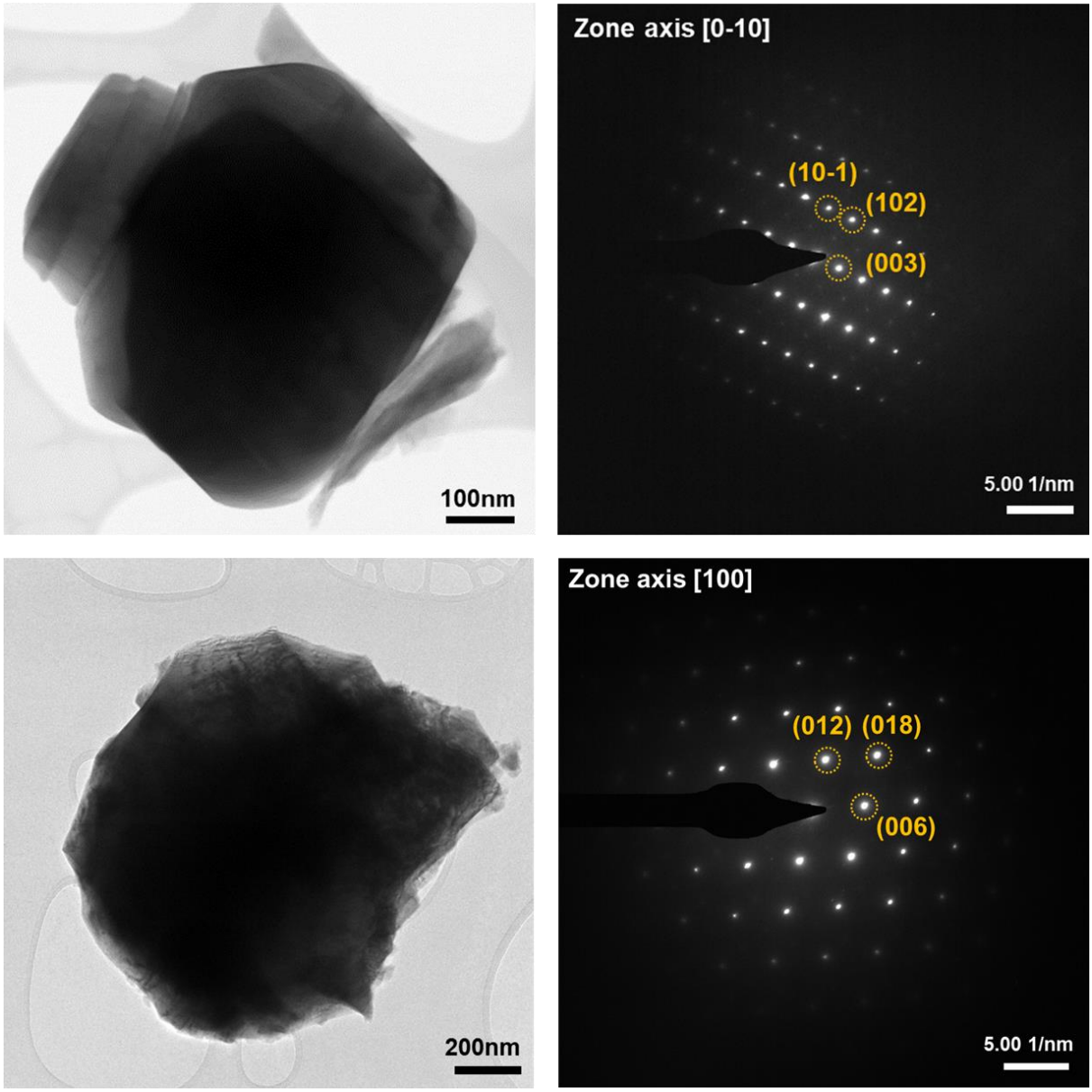

Fig. S17 TEM images and selected area electron diffraction (SAED) patterns of an upcycled NCM811.

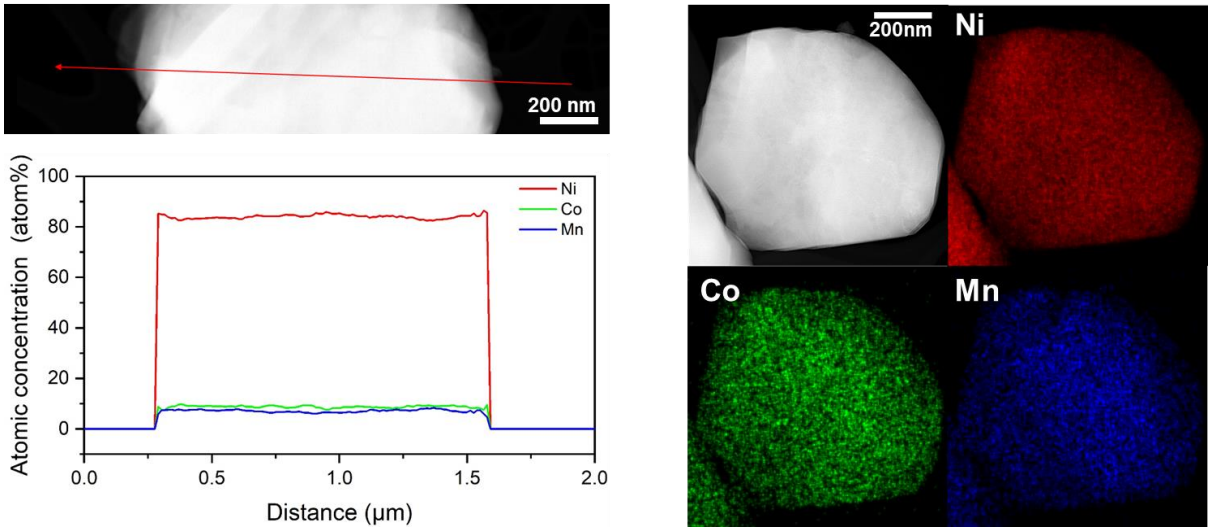

Fig. S18 Line scans of elemental profiles and elemental distribution mapping images of an upcycled NCM811 obtained using TEM-EDS.

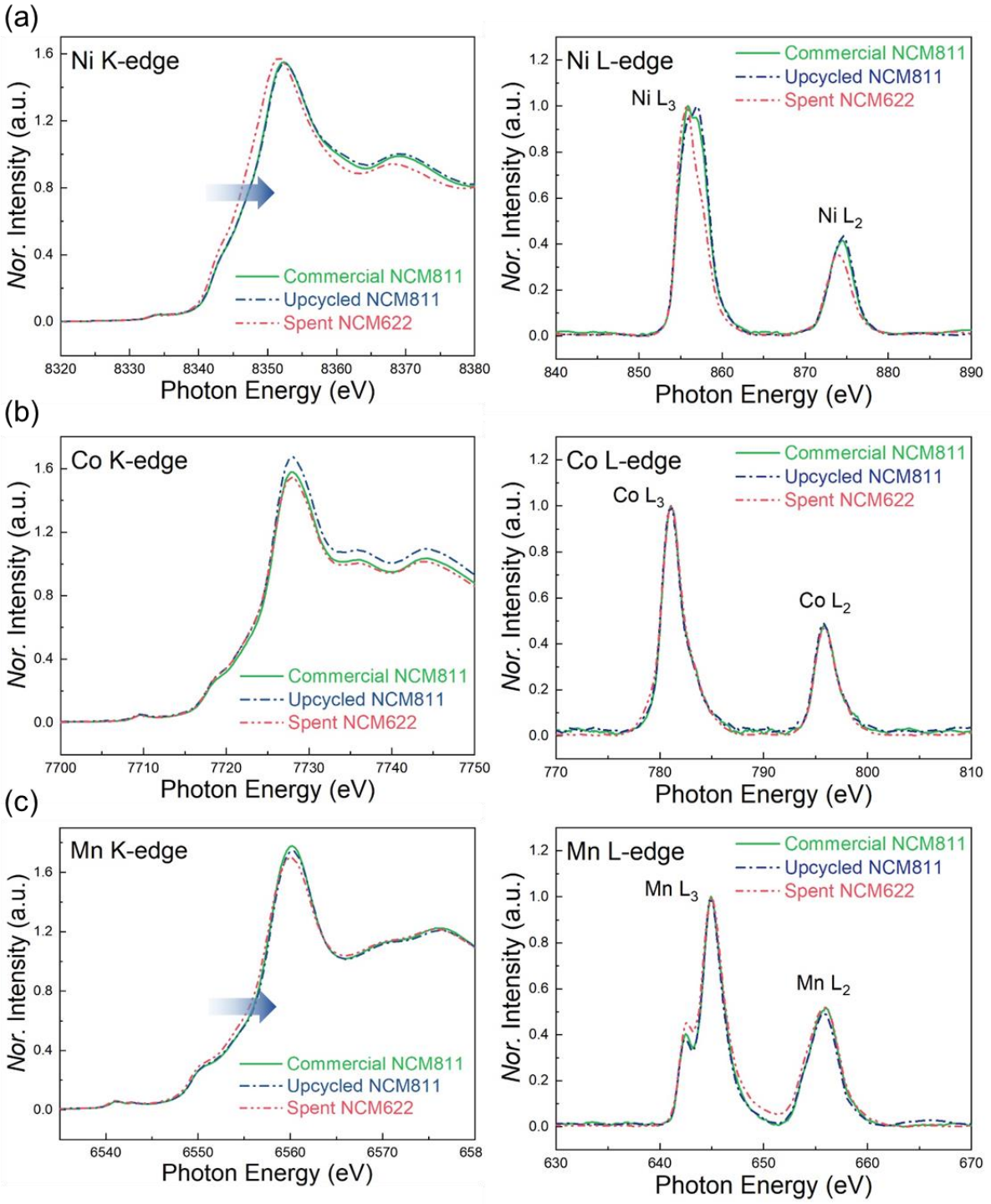

Fig. S19 XANES and soft-XAS spectra of (a) Ni K-edge/L-edge, (b) Co K-edge/L-edge, and (c) Mn K-edge/L-edge of spent NCM622, commercial NCM811, and upcycled NCM811.

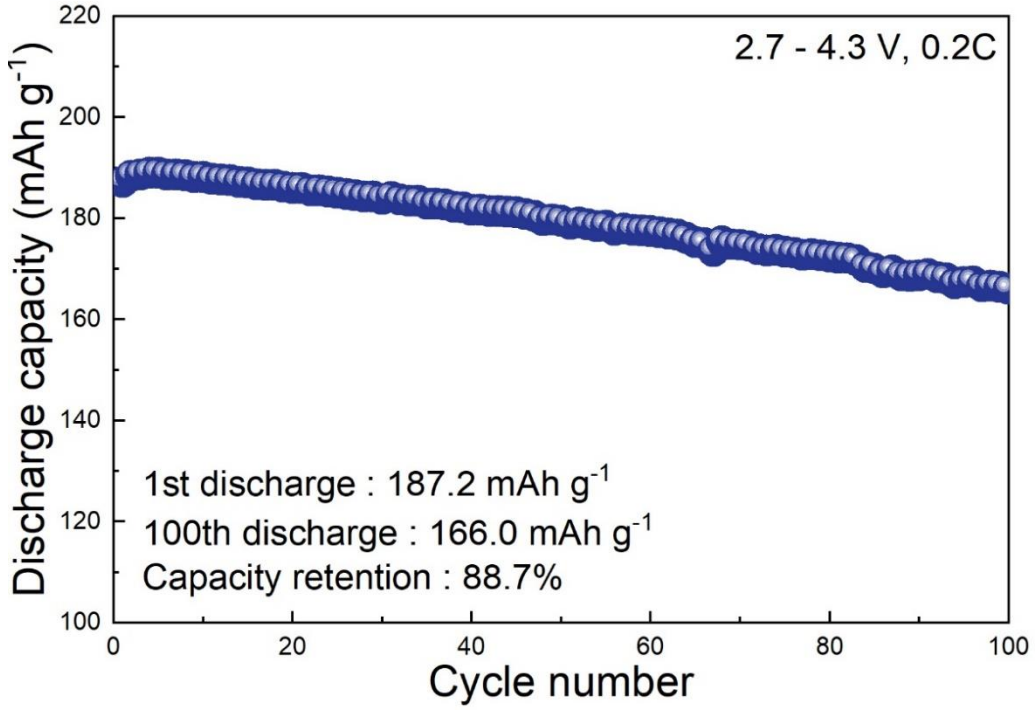

Fig. S20 Cycle performance of upcycled NCM811 at 0.2C.

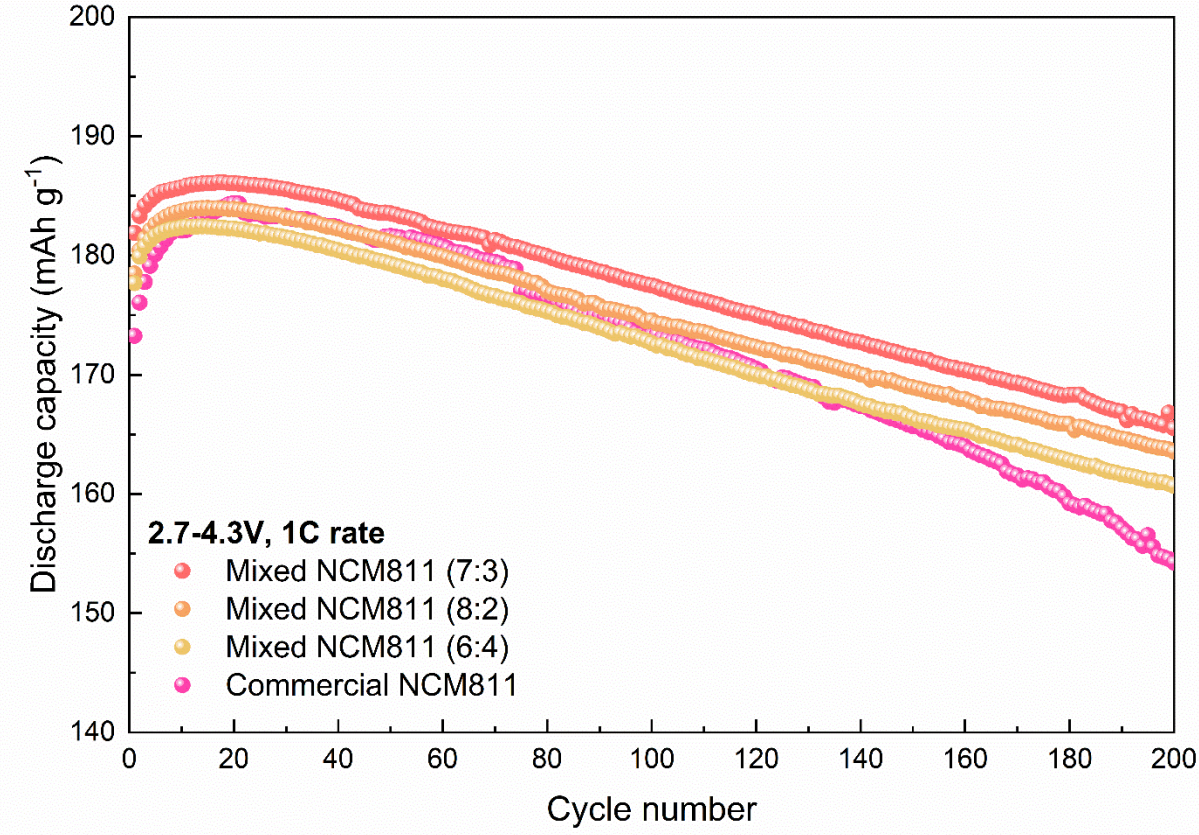

Fig. S21 Cycle performance of mixed electrodes with different cathode ratios (Commercial polycrystalline: Upcycled single-crystalline) and commercial NCM811 at 1C.

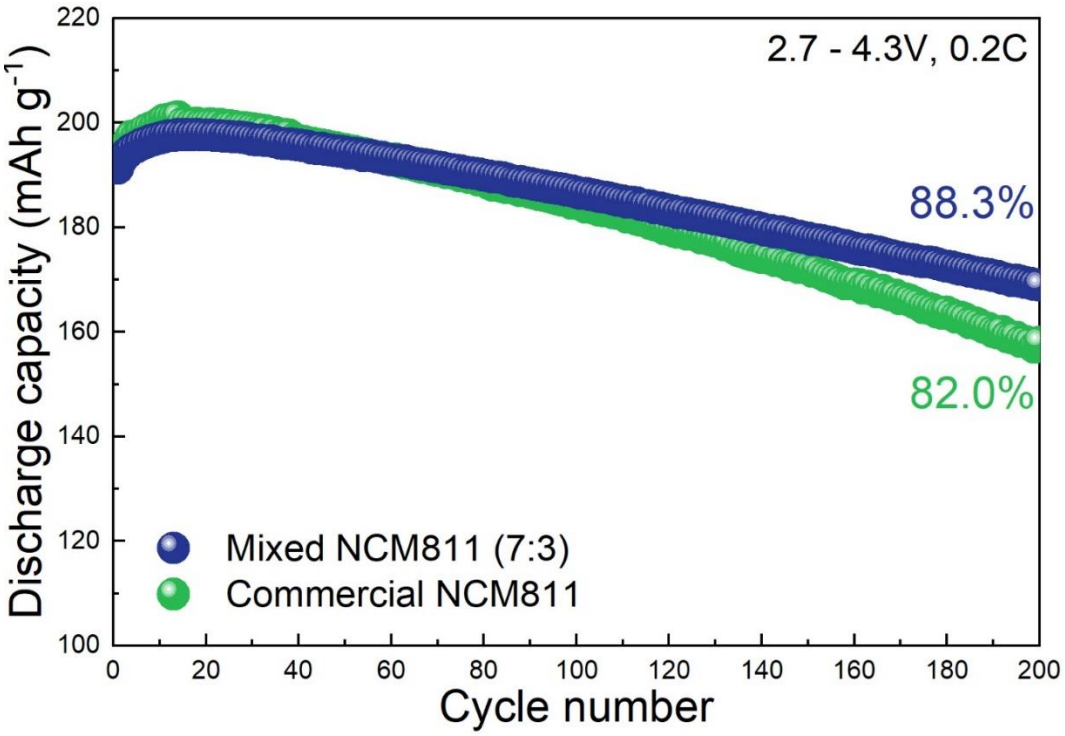

Fig. S22 Cycle performance of mixed NCM811 (7:3) and commercial NCM811 at 0.2C.

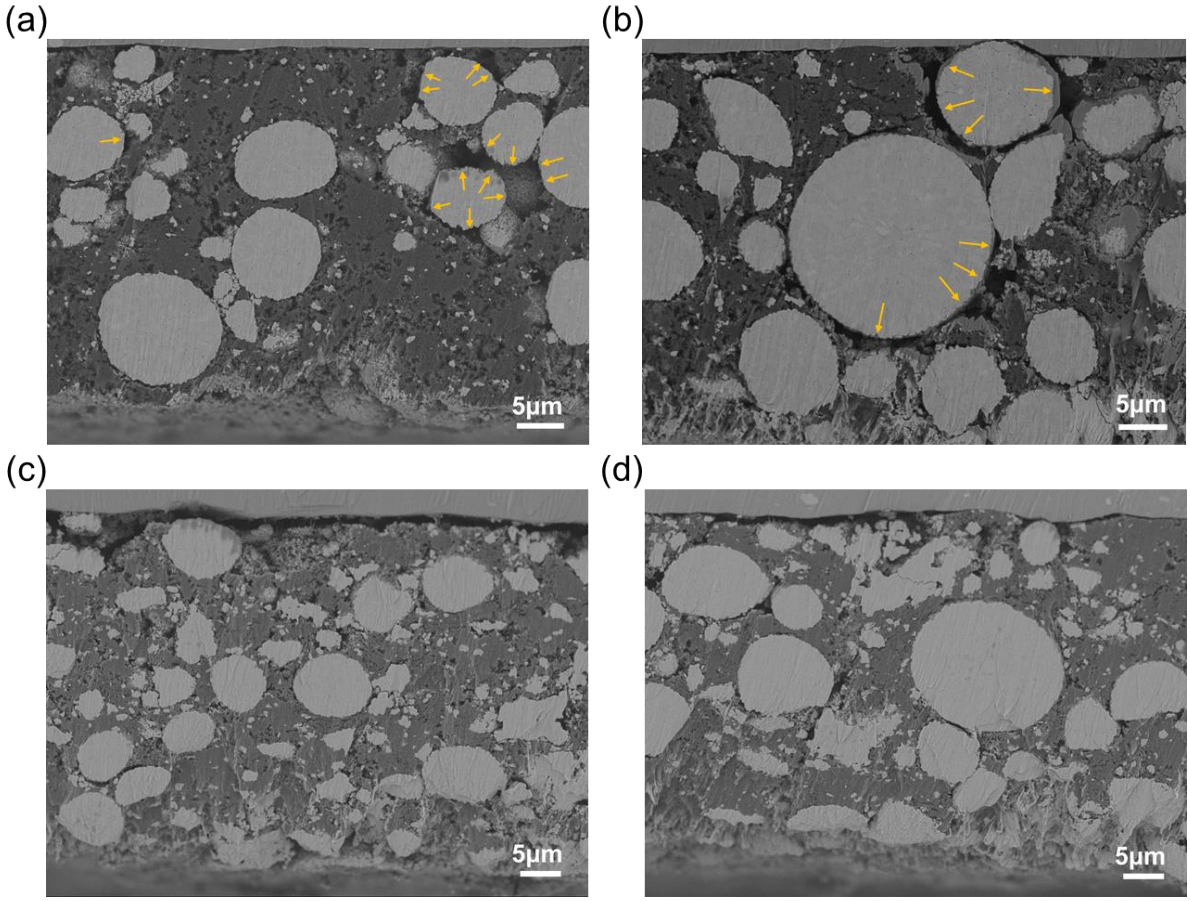

Fig. S23 Electrode cross-section images of (a, b) Commercial NCM811 and (c, d) Mixed NCM811 using SEM

Examining the cross-section of the commercial NCM811 electrode in Fig. S23a-b reveals regions marked by agglomeration of conductive material and binder, accompanied by noticeable voids around secondary particles (highlighted by yellow arrows). Such agglomerations hinder uniform electrolyte penetration, resulting in particle overcharging/discharging and poor cycle stability. In contrast, the mixed NCM811 electrode, as observed in Fig. S23c-d, exhibits evenly distributed active material, thereby inducing uniform reactions and subsequently superior cycle performance.

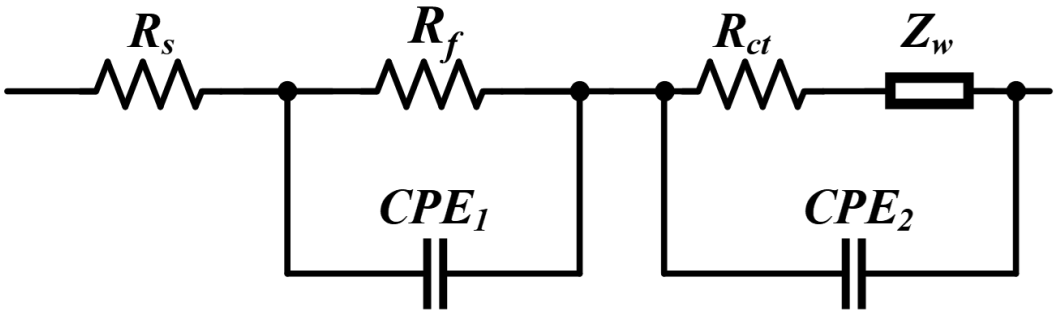

Fig. S24 Equivalent circuit used to fit and describe electrochemical impedance spectroscopy (EIS) data.

In the equivalent circuit shown in Fig. S24, R_s represents the impedance of the electrolyte and cell components, R_f represents the solid electrolyte interphase formed on the cathode surface [6], R_{ct} represents the charge transfer between the electrode and electrolyte, CPE represents the double-layer capacitance, and Z_w represents the Warburg impedance.

Sample	Cycle	R_s (Ω)	R_f (Ω)	R_{ct} (Ω)
Commercial NCM811	1st	3.211	22.784	385.068
	50th	3.090	51.047	336.548
	100th	3.324	97.907	466.773
	200th	3.912	117.623	807.151
Mixed NCM811	1st	4.221	35.515	296.449
	50th	4.234	47.611	313.101
	100th	4.401	63.012	431.048
	200th	4.465	80.651	728.466

Table S9 The fitted results from EIS data at various cycles.

References

1. X. Chang, M. Fan, C. F. Gu, W. H. He, Q. Meng, L. J. Wan and Y. G. Guo, *Angew. Chem. Int. Ed. Engl.*, 2022, **61**, e202202558.
2. X. Qu, B. Zhang, J. Zhao, B. Qiu, X. Chen, F. Zhou, X. Li, S. Gao, D. Wang and H. Yin, *Green Chem.*, 2023, **25**, 2992-3015.
3. T. A. Anufrieva, L. E. Derlyukova and M. V. Vinokurova, *Russ. J. Inorg. Chem.*, 2001, **46**, 16-19.
4. G. G. Fouga, G. De Micco and A. E. Bohé, *Thermochim. Acta*, 2009, **494**, 141-146.
5. M. J. McNallan and W. W. Liang, *J. Am. Ceram. Soc.*, 1981, **64**, 302-307.
6. P. Wang, X. Cui, D. Zhao, D. Yan, H. Ding, H. Dong, J. Wang, S. Wu and S. Li, *J. Power Sources*, 2022, **535**.